Soil Biology and Biochemistry 118 (2018) 42–50

Contents lists available at ScienceDirect

Soil Biology and Biochemistry

journal homepage: www.elsevier.com/locate/soilbio

Anoxic microsites in upland soils dominantly controlled by clay content

Marco Keiluweit[a,b,*], Kaitlyn Gee[b], Amanda Denney[b], Scott Fendorf[b]

[a] School of Earth and Sustainability & Stockbridge School of Agriculture, University of Massachusetts, 161 Holdsworth Way, Amherst, MA 01003, United States
[b] Earth System Science, Stanford University, Via Ortega 473, Stanford, CA 94305, United States

ARTICLE INFO

Keywords:
Redox gradients
Texture
Metabolic diversity
Soil carbon stabilization
Soil organic matter
Climate change

ABSTRACT

Recent evidence suggests that oxygen limitations are a critical regulator of soil organic matter mineralization rates, even within seemingly well-drained upland soils. Oxygen limitations may arise in otherwise well-aerated soils when oxygen consumption (via microbial respiration) in soil microsites outpaces oxygen supply (through diffusion). Due to analytical limitations, attempts to parameterize oxygen limitations in models have so far been limited to measures of bulk oxygen concentrations or cm-scale gradients within larger soil structural units (e.g., aggregates or peds). Smaller anoxic microsites may thus have gone undetected, limiting our ability to accurately model and predict anoxic pore volume. Here we quantify the extent of anoxic microsites in soils held at moderate moisture and identify the soil properties that dictate their formation and persistence. Using a planar optode imaging system, we monitored oxygen dynamics during incubations of a range of soils spanning natural and artificial gradients in texture and organic matter availability. While bulk oxygen concentrations ranged from 40 to 100% of saturation, we observed significant micro-scale variability resulting in the formation of anoxic microsites, here defined as soil spaces showing less than 5% saturation. Anoxic microsites comprised 2 and 9% of the total soil volume, or 14–85% of the total pore volume. Bulk oxygen concentrations showed a strong negative correlation with bioavailable organic matter, presumably due to its influence on microbial oxygen consumption. In contrast, the extent of anoxic microsites was negatively correlated to clay content, an effect attributed to limited oxygen supply in clay-rich microstructures. Our results demonstrate that texture-dependent diffusion limitations at moderate moisture conditions cause an abundance of anoxic domains, not only in cm-sized macroaggregates as current modeling approaches assume, but also within micro-aggregates. Anoxic domain size within these microstructures is at least partially decoupled from bulk oxygen concentrations, challenging the use of bulk oxygen concentrations for predicting microbially available oxygen levels and resulting OM mineralization rates and pathways in upland soils.

1. Introduction

Soil plays a critical role in global carbon (C) cycling, representing the largest dynamic C stock on Earth— 3000 Pg of C are stored in soils (Köchy et al., 2015). Soil organic matter (OM) quantities are regulated by the balance between plant inputs and losses through microbial OM mineralization (i.e., complete oxidation of organic compounds to CO_2) or export of dissolved OM in a given soil. Fundamental drivers of OM mineralization are principally climatic factors, such as temperature and precipitation, combined with OM chemistry (Cotrufo et al., 2015), C and nutrient availability (Fontaine et al., 2007; Klotzbücher et al., 2011; Torn et al., 2005), the formation of protective associations between OM and soil minerals (Oades, 1988; Torn et al., 1997), and physical protection, which constrains the accessibility of substrates to decomposer organisms (Killham et al., 1993; Veen and Kuikman, 1990). What remains elusive is how oxygen limitations in anoxic microsites, existing within otherwise well-aerated upland soil, impact overall rates of OM mineralization.

Limited oxygen supply into soil structural units (e.g., peds or larger aggregates) can promote the formation of anoxic microsites, even within seemingly aerobic, well-drained soils. Macropores (> 50 μm), with low tortuosity and high pore connectivity, in combination with micropores, with high tortuosity and discontinuity, result in highly-variable flow of gas and water (Jarvis, 2007). If oxygen diffusion through fine-textured micropore domains is slower than its consumption by microbes through respiration, oxygen is depleted and anoxic microsites are established (Sexstone et al., 1985). Interior micropore domains of soil structural units may thus become oxygen depleted relative to the exterior (macropores). Although there is abundant evidence for the existence of anoxic microsites in otherwise well-aerated upland soil (Keiluweit et al., 2016), the relative impact of diffusion limitations and oxygen consumption on the formation of anoxic

* Corresponding author. School of Earth and Sustainability & Stockbridge School of Agriculture, 161 Holdsworth Way, University of Massachusetts, Amherst, MA 01003, United States.
E-mail address: keiluweit@umass.edu (M. Keiluweit).

https://doi.org/10.1016/j.soilbio.2017.12.002
Received 14 June 2017; Received in revised form 26 November 2017; Accepted 5 December 2017
Available online 22 December 2017
0038-0717/

microsites is largely unknown.

The absence of oxygen prompts microbes to switch to alternate electron acceptors, and a diversity of anaerobic metabolic pathways transpire (Hansel et al., 2008). The lack of oxygen in permanently anoxic environments such as marine sediments (Hedges and Keil, 1995) or low-land soils (inclusive of wetlands, peatlands and rice paddies) (Megonigal et al., 2003; Reddy et al., 2000) dramatically reduces OM mineralization rates compared to aerobic environments. This rate-limiting effect is often attributed to the inhibition of oxidative depolymerization reactions (kinetic effects) (Freeman et al., 2001) or the lower energy yields associated with alternate electron acceptors used in anaerobic respiration in the absence of oxygen (thermodynamic constraints) (Arndt et al., 2013; Reddy et al., 1986). We recently showed that anoxic microsites can exert a similarly fundamental control on mineralization rates in upland soils (Keiluweit et al., 2017). In this previous study, mineralization rates in anoxic microsites were reduced by ~90% compared to well-aerated soil environments.

Traditional soil C models (e.g., DayCent and RothC) were not developed to represent the impact of soil microsite differentiation. In upland settings, soils are assumed to be completely aerobic and, hence, mineralization is presented as an exclusively aerobic process (Gottschalk et al., 2012; Parton et al., 1998). In an effort to develop more mechanistic and predictive soil C models, oxygen availability has been incorporated as a factor regulating mineralization rates. For example, Moyano et al. (2012, 2013) predict the influence of diffusion limitations on mineralization rates based on soil moisture content and soil physical properties, an approach that does not specifically isolate the effect of oxygen availability. Davidson et al. (2012) coupled mineralization rate directly to bulk oxygen concentrations, but assumed upland soils to be fully oxygenated, in effect excluding oxygen from their calculations. Further, the focus on bulk oxygen concentrations ignores the potential effects of anoxic microsites in structurally heterogeneous soils.

More recent models (e.g., Koven et al., 2013) address this problem by estimating the anoxic pore volume. Within this anoxic portion, a scaling factor is applied to account for the expected decrease in mineralization rates. The anoxic pore volume is estimated using an approximation of the classic 'aggregate model' (Arah and Smith, 1989; Arah and Vinten, 1995; Currie, 1961), which calculates the balance between oxygen diffusion (supply) into the aggregate and microbial oxygen consumption therein (demand) based on pore size distribution and water content as summarized in Keiluweit et al. (2016). However, this approach does not take into account the heterogeneity of soil structural units. For example, microbial activity (and thus oxygen consumption) is considered constant across aggregates. In fact, the 'aggregate model' predicts that anoxic microsites are restricted to mm- or cm-sized aggregates (Currie, 1961). Oxygen gradients occurring in soil microsites at smaller spatial scale are thus not currently accounted for in models.

Here we determined the anoxic volume in upland soils experimentally and examined soil factors predicting the abundance of anoxic microsites. We anticipated that soil texture (particle size distribution) couples with OM availability to regulate oxygen supply and demand, and thus the extent of anoxic microsites. To test this hypothesis, we quantified the emergence of anoxic microsites in incubations of homogenized and repacked soil cores varying in texture and C content. We used a series of upland soils with a natural gradient in texture and C content, but otherwise similar characteristics. In addition, we manipulated (i) soil texture by mixing select soils with quartz grains ground to different particle sizes (small = 25–45 μm or large = 150–250 μm) and (ii) C content by amending soil with ground root material. Soils were incubated over a 35-day period at 60% water filled pore space, a moisture content at which microbial activity is often close to maximum (Franzluebbers, 1999; Linn and Doran, 1984) and many laboratory incubations are conducted. We monitored the extent of anoxic microsites throughout the incubations using a non-invasive planar optode imaging technique, which quantifies oxygen concentrations at a spatial resolution of 1.35 μm in both air- and water-filled pores (Fig. 1). To assess the impact of anoxic microsites on anaerobic metabolism, we monitored Mn and Fe reduction rates. Finally, we quantified soil factors influencing oxygen supply (texture, porosity, pore size distribution) and demand (microbial biomass and OM bioavailability) to identify the best predictors of bulk oxygen concentrations and the anoxic pore volume.

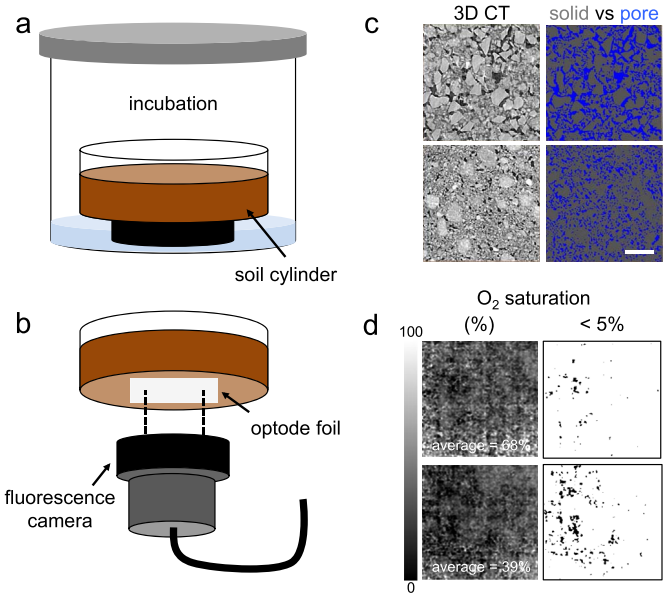

Fig. 1. Experimental approach to measuring anoxic microsites. a) Incubation setup consisting of soil cores in air-tight jars. b) Recording of oxygen distribution using planar Optode imaging of sensor foil installed at the bottom of the soil core. c) X-ray CT microtomography images to compare the physical-chemical characteristics of soils in this study; here two soils with strong contrasts in porosity are displayed. Both reconstructed grey scale images (left) and thresholded images highlighting the solid matrix versus pore space (right) are shown. It is important to note that microaggregate structures withstood sieving (lower left image). d) Examples for Optode imaging outputs showing the spatial variations in oxygen concentration (left) and the distribution of anoxic microsites, shown as black areas, using a threshold of < 5% saturation (right). 100% saturation corresponds to the oxygen concentration in fully oxygenated water. Scale bar = 250 μm.

2. Methods

2.1. Soil sampling

We chose a series of three arable soils in the Willamette Valley, OR, with natural variations in texture and C content, but otherwise similar C inputs, geochemistry and climate (temperature and precipitation). These soils have developed from stratified, silty glaciolacustrine sediments that were deposited during the late Pleistocene. The brief but intense Missoula flood events created small-scale variability among otherwise very similar parent materials, resulting in a family of soils (Willamette, Woodburn, and Amity series) with distinct variations in texture and OM contents exploited for this study. Taxonomic classification and basic characteristics of each soil can be found in Table 1. We collected top- (depth = 10–30 cm) as well as subsoil (depth 90–110 cm) material, which was sieved (< 250 μm), air-dried, and stored until further use.

2.2. Soil characterization

Particle-size distribution (texture) was determined using a particle size analyzer (Coulter® LS 230). Prior to analysis, air-dried and sieved samples were gently ground using a ceramic pestle and mortar. A 16-part spinning riffler was used to accurately create representative splits

Table 1
Physical and chemical soil characteristics hypothesized to influence anoxic pore volume.

Sample ID	Soil type	Depth	pH	Clay content	Porosity[a]	Pore radius	Tortuosity Factor	C	C/N	WEOM	POM	MAOM	Microbial biomass
		cm		%	%	μm		%	ratio	μg C g^{-1}	mg C g^{-1} soil		μg C g^{-1}
WA-20	Fine silty, mixed, superactive, mesic	20	5.1	10.7	14.5	4.58	0.4965	2.5	13.3	30.1	3.1	3.7	310
WA-100	Ultic Argixeroll	100	5.9	12.1	7.2	4.69	0.4965	0.33	8.3	4.8	0.6	0.3	100
WO-20	Fine silty, mixed, superactive, mesic	20	5.2	11.2	9.5	4.54	0.4964	1.3	15.0	47.6	4.7	2.2	222
WO-100	Aquic Argixeroll	100	5.4	13.3	9.5	4.27	0.4954	0.13	7.1	3.3	0.6	0.9	115
AM-20	Fine loamy, mixed, superactive,	20	5.2	13.1	17.1	3.73	0.4913	1.6	10.6	39.2	2.8	3.4	304
AM-100	mesic Argiaquic Xeric Argialboll	100	6.4	13.9	13.3	4.37	0.4956	0.24	7.7	5.5	0.7	0.5	131

[a] X-ray computed tomography (CT) visible porosity. A spot (voxel) size of 3.25 μm was chosen, which limits this porosity estimate to pores larger than 3.25 μm.

of 0.2–0.5 g. Samples were suspended in MilliQ water in the sample chamber and sonicated (60 s) before each analysis to further disperse particles. The particle-size distribution (4×10^{-5} mm to 2 mm) of each sample was measured at least three times and averaged.

To isolate OM of decreasing bioavailability (water extractable > particulate > > mineral-associated OM) in the untreated soil, we used a density fractionation procedure in combination with a water extraction. Briefly, two sodium polytungstate (STP) solutions were prepared in DI water at the following densities: 1.65 and 2.4 g cm^{-3} (SPT solutions #1 and #2, respectively). Particulate organic matter (POM) with a density of less than 1.65 g cm^{-3} was isolated by combining 5 mL of SPT solution #1 with 1 g of untreated soil in a 15 mL falcon tube, mixing for 30 s on a vortexer, and shaking for 2 h at 120 rpm. The suspension was then centrifuged at 4000 × *g* for 30 min. The supernatant was filtered (Whatman GF/F, 0.45 μm pore size) and rinsed with 40 mL of DI water to remove residual SPT. This process was repeated twice on the residual pellet to ensure that all material with a density lower than 1.65 g cm^{-3} was collected. To separate mineral-associated organic matter (MAOM) with a density > 2.4 g cm^{-3}, the remaining pellet was resuspended in SPT solution #2 and subsequently treated as described for POM. Filters were rinsed with DI water to collect the sample material, frozen in liquid nitrogen and freeze-dried. Water-extractable organic matter (WEOM) was determined by combining 1 g of soil and 10 mL DI water, vortexing for 30 s, and placing the slurries on a shaker for 1 h at 120 rpm. The mixed solution was then centrifuged at 4000 × *g* for 30 min. The supernatant was filtered through 0.2 μm membranes and stored at 4 °C until further analysis Initial C and N contents for bulk soil and density isolates were measured by combustion (Carlo Erba NA 1500 analyzer), while WEOM was quantified on a TOC analyzer (Shimadzu TOC-5000A).

2.3. Texture and OM content manipulations

In addition to utilizing the natural variations in texture, C content, and OM availability in our soils, we manipulated both factors in separate treatments. To induce a texture gradient, Woodburn top- and subsoil material were mixed at a 1:1 (dry wt.) ratio with acid-washed quartz sand sieved to 25–45 or 150–250 μm particle size. In the following, texture treatments are referred to as small, S, and large, L, respectively. The coarse texture treatment showed a larger porosity (+17 and + 74%) and smaller clay content (−18 and −21%) in top and subsoils, respectively, compared to the fine texture treatment. To vary OM availability, Woodburn top- and sub-soil were amended with 1 wt. % finely ground root material (*Avena sativa*) as a proxy for POM. POM additions increased WEOM by 10 and 70% in top and subsoil, respectively.

2.4. Incubation experiments

Both untreated soils and soil amended with quartz or roots were packed in perforated cylinders (diameter = 4.7 cm, height = 0.8 cm) at the same bulk density (1.3 g cm^{-3}, average of field bulk density of all soils) and brought to 60% water-filled pore space. Cylinders were covered with gas-permeable Parafilm to minimize moisture loss. Soils were then incubated at room temperature for 35 days in canning jars. Jars were vented twice a day during the first day, and once a day during the remainder of the incubation period to maintain headspace CO_2 concentrations below 1%. Gas chromatographic measurements of headspace oxygen concentrations indicated that headspace concentrations were not affected by oxygen consumption in the soil (data not shown). At each sampling point, soil within the incubation jar was checked for moisture loss, which was less than 1% over the duration of the experiment.

2.5. Mineralization rates

CO_2 and CH_4 production in the headspace was measured at multiple time points through the incubation period. Incubation jars were closed preceding sampling to allow for gas accumulation. Gas samples were extracted from the headspace (10 mL) and measured by gas chromatography (Shimadzu GC-2014). After each measurement, samples were vented for 10 min. Mineralization rates were calculated using an initial concentration as determined by control samples at time of closure and assuming constant production/consumption rates during the incubation period. A selection of kinetic models were fitted to the data to identify the one that best presents our observed mineralization kinetics (Sleutel et al., 2005). A parallel first-order and zero-order model (Kessel et al., 2000) resulted in the best fit and was used to derive rate constants and pool sizes. This model assumes that OM consists of an easily degradable (fast-cycling) C pool that is mineralized exponentially according to first-order kinetics, and a slow cycling fraction that is mineralized according to zero-order kinetics. The amount of mineralized carbon, C, at any time, t, is:

$$C(t) = C_f\{1 - \exp(-k_f t)\} + k_s t \quad (1)$$

where k_f is the mineralization rate constant of the fast-cycling C pool C_f, and k_s is the mineralization rate constant of the slow cycling pool. All curves were fit to cumulative data of CO_2-C with OriginPro 10 as unconstrained non-linear regressions by the Levenberg–Marquardt algorithm.

2.6. Spatial visualization of oxygen distribution

To visualize the distribution and concentration of oxygen, a planar optode imaging system (VisiSens 2, PreSens Precision Sensing GmbH, Germany) was used. In addition to determining oxygen distribution at a pixel size of 1.35 μm (enabled by Adaptor Tubus 3, PreSens Precision Sensing GmbH, Germany), the planar optode system is capable of detecting oxygen in both water- and air-filled pores. The system consists of a light-emitting camera, O_2-sensitive fluorescent foils, and an image processing software. The camera records the resultant emission signal from the fluorescent films, which were adhered to the inner and bottom

surface of the incubation cylinders. Triplicate cylinders equipped with the film were packed with soil and incubated as the described for the respiration measurements above. At multiple time points throughout the incubation period the cylinders were removed from the incubation jar and mounted on the camera setup. The spatial distribution of O_2 was then mapped over the total area of the film based on the relative intensities of the excitation and emission light signals. To convert the relative intensities of excitation and emission signals to oxygen saturation, a two-point calibration was conducted in the incubation cylinder filled with oxygen-saturated DI H_2O (100% saturation) and an anoxic standard solutions (0% saturation) as described by the manufacturer. Using this calibration, bulk oxygen concentrations were computed in the complementary software (VisiSens AnalytiCal 1, PreSens Precision Sensing GmbH, Germany), which assumes Stern-Volmer kinetics for fluorescent O_2 quenching. Calibrated images were transferred into ImageJ, a public domain imaging software, where the anoxic area was computed as the proportion of the total image area with less than 5% of saturation. This value was chosen as the cutoff because experiments with fully aerated soil and entirely anoxic soil indicated a 5% error for the planar optode imaging analysis. It is important to note that optode measurements detect oxygen in both the aqueous and gas phase. Oxygen concentrations are therefore presented in units of "% air saturation", a convention recommended by the manufacturer and practiced in other optode studies (Elberling et al., 2011; Haberer et al., 2011). Additional measurements with oxygen micro-electrodes (Clark-type, Unisense, Denmark) confirmed the absence of oxygen gradients with depth across the soil column (from surface of soil to optode foil), indicating that the values recorded by optode at the bottom of the cylinder are representative for the entire soil volume.

2.7. Anaerobic metabolism and OM availability

To monitor anaerobic microbial activity and OM availability, Mn (II), Fe(III) and WEOM concentrations were determined at multiple time points throughout the incubation. Triplicate cylinders were harvested and transferred into an anoxic glove bag, where they were air-dried for 2 days. Dry samples were then extracted with MilliQ-purified water, 2 M KOH or 0.5 M HCl (1:10 soil-solution ratio) for one hour in the dark, centrifuged at 4000 × *g* for 15 min, and the supernatant was filtered through 0.2-μm syringe filters. At each time point, concentrations in the water extracts were determined as described above. We assumed that HCl-extractable Mn, which was quantified by ICP (Thermo Scientific ICAP 6300 Duo View Spectrometer), predominantly represents Mn(II). Fe(II) was measured using the Ferrozine assay (Stookey, 1970).

2.8. X-ray tomography and reconstruction

To provide quantitative measures for the pore structure, soils were scanned using the X-ray micro-tomography beamline 8.3.2 at the Advanced Light Source (Lawrence Berkeley National Laboratory, United States) (MacDowell et al., 2012). Transmitted X-ray light is converted to visible light using a $CdWO_4$ single crystal scintillator, magnified by a Canon 2X lens, and imaged using the OptiquePeter (OP) optics system and PCO.Edge CCD camera. The incident beam was tuned to 30 keV to provide optimal transmission. In this setup, the resulting image pixel size was 3.25 μm and the field of view 8.3 mm. Natural soils and artificial treatments were packed, wetted and incubated as described above, but in this case smaller plastic cylinders (diameter = 0.6, height = 0.8 cm) were used to allow for sufficient X-ray transmission. Sample cylinders were scanned in continuous mode, acquiring a set of 1440 transmission images while rotating the sample by 0.125° for each scan. The resulting image stacks were reconstructed and processes using the ImageJ plugin Fuji in multiple steps: (1) selection of a region of interest (ROI) without boarder artifacts, (2) reconstruction and ring removal, (3) application of a median filter, and (4) grey value threshold segmentation based on inspection of the histograms. ROI selection, reconstruction and ring removal was done using the ALSuCT-recon function developed by the A:S. After inspection of the histograms of samples, a single threshold was chosen for the segmentation of all datasets. Porosity was computed in Avizo 9.0 (Visualization Science Group, Inc., Burlington, MA) using the morphological *Opening* operator assuming cubic openings with a kernel size of 1. Our X-ray CT analysis underestimates porosity due to the relatively large spot size chosen for the imaging analysis, which prevented us from accounting for pores smaller than 3.25 μm. We therefore refer to our porosity estimate as "X-ray CT visible porosity" in the following. Pore size distribution was obtained by applying the Local Thickness function within the BoneJ plugin (Doube et al., 2010) to the segmented data as described in Bacher et al. (2015). The Local Thickness function utilizes Euclidean distance transforms to analyze 3D images by fitting spheres of maximal radii in void spaces, here represented by air- or water-filled pores. Geometric mean pore volume was computed using pore size distribution and tortuosity factors were calculated as described by Nielson et al. (1984).

2.9. Correlation analysis and statistics

A first linear correlation analysis was performed between bulk oxygen concentration or anoxic volume on days 13 and 35 of the experiment and soil characteristics hypothesized to influence oxygen transport (clay content, porosity, mean pore size, and tortuosity) or oxygen consumption (C content, C/N, WEOM, POM, MAOM, and Microbial biomass C). A second linear correlation analysis was performed between respiration rates, WEOC concentration, and bulk oxygen concentrations at each time point during the incubation. Pearson's correlations were carried out using the Levenberg–Marquardt algorithm in OriginPro (OriginLab Cooperation, Northampton, MA).

3. Results

3.1. Soil characteristics

Soils varied in clay content, X-ray CT visible porosity, C content, WEOM, and POM, and microbial biomass C, with top (20 cm) and subsoils (100 cm) showing greater differences than the intra-depth variations between soils (Table 1). Among the measured chemical properties, differences in C content were the most pronounced, whereas X-ray CT visible porosity showed the greatest variation among the physical properties tested.

3.2. Microbial respiration

As expected, we observed higher mineralization rates (and thus microbial respiration) in topsoils than subsoils (Table 2). Total mineralized C at the end of the incubation period (C_{min}) was positively correlated with total C content (R^2 = 0.95, $P < 0.05$). Mineralization rates were highest at the beginning of the incubation period (days 1–13) and subsequently decreased (Fig. 2). Over the full incubation period, soil-specific mineralization rates at each time point were negatively related to the amount of WEOM (R^2 = 0.36–0.63), which sharply declined within the initial incubation period and subsequently recovered (Fig. 3a). In order to quantify and compare mineralization rates during initial and late periods, rate coefficients were obtained based on fits obtained with a first- and zero-order kinetic model, which divides OM into a fast and a slow cycling pool (Table 2). The rate coefficient for slowly decomposing C (k_s) trended negatively with WEOM and POM (R^2 = 0.68 and 0.65, $P > 0.05$). POM additions increased C_{min} and C_f, while finer particle size caused a small yet notable decrease in the mineralization of both pools. These results suggest that C content and availability had a strong influence on microbial respiration (and thus oxygen consumption).

Table 2
Rate parameters for OM mineralization as well as Mn and Fe reduction.

Soil	C_{min}	C_f	k_s	k_f	$R_{Mn\ reduction}$	$R_{Fe\ reduction}$
	μg C g^{-1}	μg C g^{-1}	d^{-1}	μg C g^{-1} d^{-1}	μg Mn(II) g^{-1} d^{-1}	μg Fe(II) g^{-1} d^{-1}
a) Natural soils						
WA20	1670	2084	6.8E-13	0.048	1.7	12.7
WA-100	196	149	1.4E+00	0.094	0.3	12.1
WO-20	680	795	1.5E-14	0.055	2.2	13.0
WO-100	260	175	2.4E+00	0.108	0.8	5.5
AM-20	872	1063	3.4E-13	0.050	4.5	16.5
AM-100	235	214	8.3E-01	0.833	0.7	8.3
b) POM amendments						
WO-20 + POM	1696	1349	1.1E+01	0.134	n.a.	n.a.
WO-100 + POM	1065	815	7.5E+00	0.154	n.a.	n.a.
c) Texture manipulations						
WO20 + L	49	702	7.2E+01	0.472	n.a.	n.a.
WO20 + S	51	580	6.6E+01	0.311	n.a.	n.a.
WO100 + L	16	823	2.0E-14	0.039	n.a.	n.a.
WO100 + S	18	4	3.9E+00	47.00	n.a.	n.a.

+POM = soil amendments with particulate organic matter consisting of root material.
+L and +S = texture manipulations consisting of quartz grains ground to small (+S; 25–45 μm) and large (+L, 150–250 μm) particle sizes mixed with soil at a 1:1 ratio (wt.).
C_{min} = total mineralized C at the end of incubation experiment.
C_f = size of fast cycling C pool.
k_f = first-order rate constant of the fast cycling C pool.
k_s = zero-order rate constant of the slow cycling C pool.
f_{anoxic} = area percent with less than 5% oxygen saturation.
$R_{Mn\ reduction}$ = Mn(II) production rate in the initial incubation period (day 1–13).
$R_{Fe\ reduction}$ = Fe(II) production rate in the initial incubation period (day 1–13).

3.3. Evidence for anaerobic metabolism

Measurable rates of Mn and Fe reduction suggest a notable contribution of anaerobic metabolism to overall OM mineralization. As Mn (II) and Fe(II) production increased most strongly during the initial stages of incubation (days 1–5) (Fig. S-1), we were able to calculated Mn and Fe reduction rates (Table 2). Rates were greater in the topsoils than in the subsoils, and with finer particle size in the texture treatment. Results for the POM treatment showed no systematic trend (data not shown), possibly due to the interference of POM with metal extractions. Combined, these results indicate that the contribution of Mn and Fe reduction to overall C mineralization is greater in C-rich topsoils during periods of strong microbial activity.

3.4. Bulk oxygen dynamics and anoxic volume

In general, the observed oxygen dynamics mirror the patterns in microbial respiration described above. Bulk oxygen concentrations decline during the initial incubation period (day 1–13) and recover during the later stages of the incubation (Fig. 3b). Bulk oxygen concentrations in topsoils (66 ± 6% saturation) were significantly lower than in subsoils (86 ± 6%) when averaged across the experimental period ($p < 0.001$). The addition of POM further (and significantly) decreased average concentrations to 45 ± 6% in the topsoil and 46 ± 6% in the subsoil ($p < 0.001$), while texture manipulations showed no significant effect (data not shown). The anoxic volume was low within the first few days, reached a maximum on day 13, and declined again thereafter (Fig. 3c). The anoxic volume of the total soil volume (sum of pore space and solids) ranged between 2 and 9% (day 13) in the earlier and 2–7% (day 35) in the later stages of the incubation. POM additions increased anoxic volume by a factor of 1–6 relative to unamended soils, while texture manipulations showed up to 6-times greater anoxic volumes in the fine texture compared to the coarse texture treatment (Table S-1). The average area of individual, discrete anoxic microsites ranged from 727 to 12,500 μm^2 (corresponding to a diameter of 30–126 μm, assuming spherical geometry), but the size distribution of anoxic microsites did not change significantly depending on soil type or treatment (Table S-2). These temporal trends suggest that bulk oxygen concentrations are directly coupled to microbial activity, but values imply well-aerated conditions even during peak microbial activity. Nevertheless, a significant share of the pore volume was found to be anoxic within soils held at modest moisture content, and the anoxic pore volume was expanded by the addition of POM or with finer texture.

3.5. Relationships between oxygen concentrations, anoxic volume, and soil characteristics

While bulk O_2 and anoxic volume roughly mirrored one another over the incubation period, bulk oxygen concentrations was a poor predictor of anoxic pore volume within individual soils ($p >> 0.05$, Fig. 3d). To assess which soil properties (Table 1) influence bulk oxygen concentration and anoxic pore volume, we performed a multiple linear regression analysis for values recorded on days 13 and 35 of the incubation. At the earlier time point (day 13), WEOM was the only factor that significantly correlated with a decrease in bulk oxygen concentrations ($R^2 = 0.69$, $P < 0.05$) (Table 3). On the other hand, clay content was the only factor that significantly correlated with anoxic volume during the initial incubation period ($R^2 = 0.68$, $P < 0.05$). These trends generally held at the later time point (day 35), although correlations were not significant at the $P < 0.05$ level. These results suggest that distinctly different soil properties govern bulk oxygen concentration and anoxic pore volume. WEOM appears to regulate bulk oxygen concentrations, whereas clay content controls the anoxic volume, especially during periods of increased mineralization.

4. Discussion

We examined the impact of texture and OM availability on the extent of anoxic microsites formed under moderate moisture conditions characteristics of many upland soils. To that end, we conducted incubations of soils with natural gradients in C content and texture, soils amended with POM, and soils subjected to texture manipulations. Bulk oxygen concentrations and the abundance and distribution of anoxic

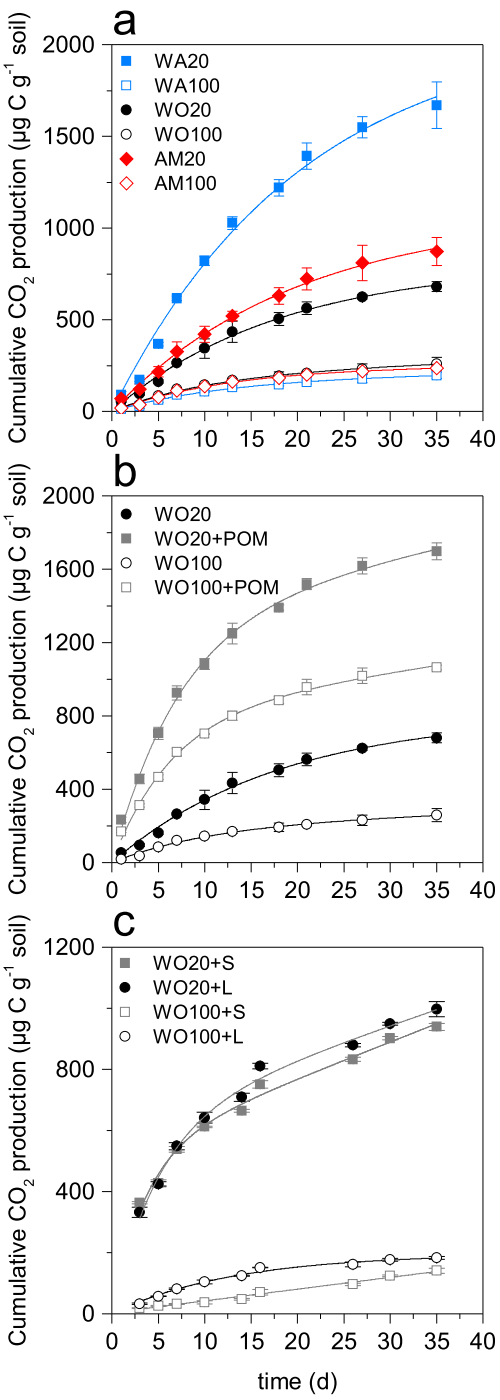

Fig. 2. Cumulative soil respiration over 35-day incubation period in (a) unamended soils, (b) organic matter additions, and (c) texture manipulations. Particulate organic matter consisted of ground root material. Texture was manipulated by mixing soil with either large (L = 150–250 µm) or small (S = 25–45 µm) inert quartz grains at a 1:1 ratio. Solid lines represent model fits using a parallel zero- and first-order kinetic model (Sleutel et al., 2005). The adjusted R^2 values of the fits were greater than 0.98 in all cases except for WO100 + L (0.977). Error bars represent standard error of three replicates.

microsites were monitored over the course of the incubations. We hypothesized that in soils held at constant, moderate moisture content, a significant fraction of the pore volume remains devoid of oxygen. We further expected that oxygen availability and the size of anoxic microsites would be regulated by the interaction of soil texture and OM availability.

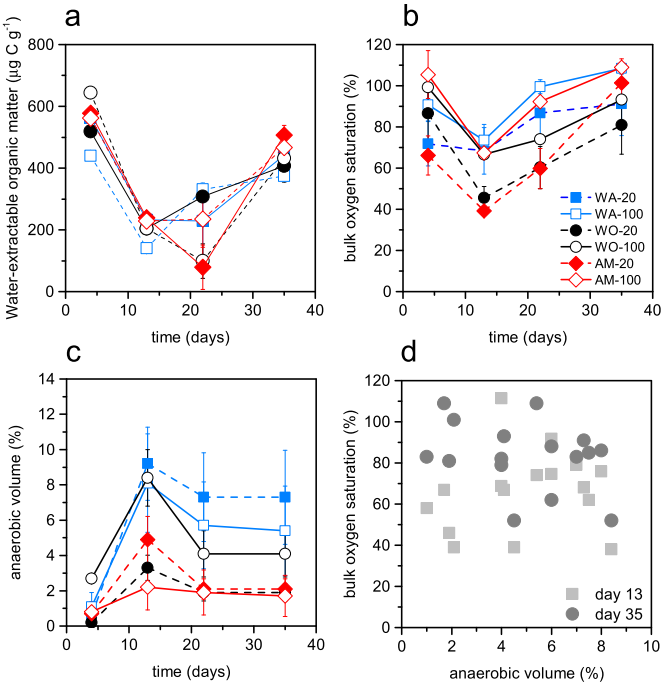

Fig. 3. Changes in (a) water-extractable organic matter, (b) bulk oxygen saturation, (c) the anoxic volume (determined using the < 5% saturation cutoff) over the full incubation period. As detailed in the methods, 100% saturation corresponds to the oxygen concentration in fully oxygenated water. (c) The relationship between bulk oxygen concentration and anoxic volume at two time points. Error bars represent standard error of three replicates.

4.1. Anoxic microsites persist at moderate moisture content

Previous efforts to quantify the anoxic fraction of upland soils have focused on oxygen gradients between the exterior of larger (cm-scale) aggregates or peds and their interior. This pioneering work relied on glass microelectrode (Clark-type) that only provide robust measurements under saturated conditions in one dimension (Leffelaar, 1988; Sexstone et al., 1985). Because the planar optode approach offered the benefit of recording both aqueous and gaseous oxygen concentration, we were able to resolve anoxic microsites under unsaturated conditions. We found that even in well-aerated soils with bulk oxygen concentrations ranging from 46 to 86% saturation, between 2 and 9% of the pore volume is under anoxic conditions (Fig. 3a and b). The presence of anoxic microsites was further supported by evidence for anaerobic respiration, specifically Mn and Fe reduction (Table 2), which is in good agreement with abundant reports of anaerobic metabolism occurring in seemingly well-drained soils (Keiluweit et al., 2016).

Because soils were homogenized to disrupt soil macrostructure, our reported values are most representatives of the micropore domains within aggregate/ped interiors. Here it is important to note that our two-dimensional planar optode approach provided relative areas, not volumes, within these micropore domains. The reported values for anoxic volumes (2 and 9%) are therefore a reflection of the percentage of the total imaged area that is anoxic. To calculate actual anoxic pore volume, total porosity would have to be taken into account. X-ray CT visible porosity in our soils ranges from 7 to 14% (Table 1). If we normalize the anoxic volume by the total porosity (= anoxic volume/total porosity × 100), we can obtain the actual anoxic pore volume, which would range from 14 to 85%. For intact soils, this calculation likely overestimates anoxic pore volume as sieving destroyed macroporosity, which would be expected to contribute to soil aeration. But they convey that a volume fraction significantly greater than 2–9% may exhibit anaerobic conditions within soil micropore domains.

Table 3
Pearson's correlation coefficients (r) for soil characteristics and oxygen concentrations or anoxic volume.

Soil properties	Bulk O_2 concentration				Anoxic volume			
	13 days		35 days		13 days		35 days	
	r	p-value	r	p-value	r	p-value	r	p-value
a) Properties influencing oxygen supply (transport)								
Clay content	-0.33	0.52	0.28	0.60	**0.82**[a]	**0.04**[a]	0.75	0.08
Porosity	-0.46	0.36	0.10	0.87	-0.55	0.26	-0.60	0.21
Pore radius	0.67	0.14	-0.14	0.79	0.35	0.51	0.47	0.35
Tortuosity	0.69	0.14	-0.22	0.66	0.17	0.76	0.28	0.59
b) Properties influencing oxygen demand (consumption)								
Total C	-0.37	0.47	-0.47	0.35	-0.17	0.76	-0.14	0.77
C/N	-0.17	0.72	-0.33	0.53	0.37	0.46	0.45	0.37
WEOM[b]	**-0.83**[a]	**0.04**[a]	-0.68	0.14	0.10	0.88	-0.10	0.88
POM[c]	-0.70	0.12	-0.77	0.07	0.10	0.84	-0.03	0.95
MAOM[d]	-0.57	0.24	-0.49	0.33	-0.26	0.6	-0.32	0.56
Microbial biomass C	-0.69	0.12	-0.17	0.75	0.40	0.43	0.17	0.73
Easily degradable C (C_f)	-0.22	0.67	-0.44	0.38	-0.30	0.57	0.24	0.63

[a] r values highlighted in bold are statistically significant at the $P < 0.05$ level.
[b] WEOM = water extractable organic matter.
[c] POM = particulate organic matter.
[d] MAOM = mineral-associated organic matter.

4.2. Bulk oxygen dynamics are regulated by OM bioavailability

The significant statistical relationship between WEOM and bulk oxygen concentrations across the entire set of soils (Table 3) suggests a strong link between bulk oxygen and mineralization of bioavailable OM. This link is further corroborated by the fact that oxygen concentrations over the incubations period tracked increases in mineralization rates and decreases in WEOM (Fig. 3a). The fact that WEOM declined during the period of high mineralization suggests that microbial utilization of bioavailable C pools (and the associated oxygen consumption) was the primary regulator of bulk oxygen concentrations during that time. Furthermore, POM additions conducted to test the effect of bioavailable OM had a substantial impact on bulk oxygen concentrations. POM additions not only increased the supply of WEOM, but also lowered average oxygen concentrations by ~22% in top- and 47% in subsoils. Depolymerization and solubilization of the added POM likely increased the amount of OM available for microbial respiration (and oxygen consumption) during the incubation. Combined, these observations indicate that OM availability – by virtue of regulating microbial respiration – is the primary control on bulk oxygen availability in our system.

4.3. Anoxic microsites emerge within diffusion-limited domains

To our surprise, bioavailable OM did not significantly affect the extent of anoxic microsites within the unamended soils (Table 3). Instead, the anoxic volume was most strongly correlated with clay content. Our texture manipulations further confirmed that finer particle size increase anoxic volume (Table S-1). Assuming spherical dimensions, the mean diameter of the anoxic microsites ranged from 30 to 126 μm (Table S-2). This size range matches that of microaggregates remaining intact even after sieving as evidenced by CT scans (Fig. 1). Clay sized particles are thought to be the building blocks of such microaggregates (Lehmann et al., 2007), and soils with greater clay content can be expected to have a greater content of microaggregates (Denef et al., 2004; Plante et al., 2006; Totsche et al., 2017). The micropore network within these clay-rich microaggregates are characterized by greater tortuosity and water retention (Zhuang et al., 2008), which are expected to lower effective diffusion rates. Diffusion constrains on the resupply of oxygen into microaggregates thus appear to be leading to the formation of anoxic microsites in our system. The formation persistence of anoxic microsites through time, especially in relation to the turnover dynamics of microaggregates (Totsche et al., 2017), thus warrants further research.

4.4. Controls on soil oxygen availability are scale-dependent

Our results suggest the emergence of anoxic microsites is partially decoupled from bulk oxygen availability. In our system, bulk oxygen concentrations decreased with increasing amounts of bioavailable OM. Microbial biomass and activity is often greatest in macropores because of the relative abundance of bioavailable OM (Bundt et al., 2001). Water extractions likely preferentially extract OM from macropores. In spite of sieving the soils before starting the experiment, macropores are clearly noticeable between microaggregates (micropore domains) in our CT scans (Fig. 1c). It thus appears plausible that microbial oxygen consumption within macropores, fueled by the supply of bioavailable OM, regulated bulk oxygen concentrations. The formation of anoxic microsites in microaggregate domains likely only has negligible impacts on bulk oxygen concentrations due to their small volume. For instance, an increase of anoxic volume from 2 to 7% in an otherwise fully aerated soil would decrease bulk oxygen concentrations only from 98% to 93%. Bulk oxygen concentrations in our system therefore appear to be primarily controlled by microbial activity and the associated oxygen consumption in macropores.

On the other hand, we found that the extent of anoxic microsites is positively related to clay content. In our system, microaggregates that withstood sieving are clearly visible in the CT scans, and they are characterized by micropore domains likely to impact effective diffusion rates (Fig. 1c). Because clays are integral building blocks for the formation of microaggregates, our results suggest that anoxic microsites form within these diffusion limited domains. While OM bioavailability and associated oxygen consumption seem to regulate bulk oxygen concentrations in macropores, oxygen concentration within micropore domains appears to be most strongly regulated by the rate of oxygen transport via diffusion. The fact that bulk oxygen concentrations and the extent of anoxic microsites are controlled by different factors suggests that the controls on oxygen availability in moderately moist soils are scale-dependent.

4.5. Implications

The finding that upland soils generally perceived as well-aerated harbor persistent anoxic microsites has important implications for

questions related to nutrient and C cycling. For example, anaerobic metabolism within these microsites can impact denitrification rates (Myrold, 1988; Sexstone et al., 1985) or nitrous oxide emissions (Bateman and Baggs, 2005). In addition, oxygen limitations are increasingly recognized as regulators of OM mineralization rates in upland soils (Hall and Silver, 2015; Keiluweit et al., 2016; Sierra et al., 2015). In fact, anoxic microsites established within the soils used in this study have recently been demonstrated to decrease OM mineralization rates by ~90% (Keiluweit et al., 2017). The observation that anoxic microsites appear to form within microaggregates also raises interesting questions regarding the mechanisms of OM protection within microaggregates, which are often thought to contribute to long-term C storage. It is often assumed that restricted microbial access to C substrates in microaggregates is the primary protection mechanism (Denef et al., 2004; Nie et al., 2014; Six et al., 2004). We highlight that anaerobic conditions are additional controls on mineralization rates within such microaggregate domains, and so may enhance C accumulation.

Our results further imply that consideration of anoxic microsites could improve model predictions of oxygen availability in well-drained upland soils. Because upland soils are generally perceived as well-drained and thus fully aerated, anoxic microsites at the scale reported here (and associated impacts on biogeochemical cycles) are not accounted for in traditional (Gottschalk et al., 2012; Parton et al., 1998) and more recent, process-based soil C models (Koven et al., 2013; Moyano et al., 2013; Riley et al., 2014). Mechanistic models, which currently rely on approximations (adapted from Arah and Vinten (1995)) to estimate anoxic volume that only capture sites within larger, mm-scale (macro)aggregates might benefit from the representation of anoxic microsites that exist at the sub-mm scale even at moderate moisture. Further, our study indicates that modeling attempts to represent oxygen dynamics in truly *micron-sized* anoxic soil environments might have to consider that controls are scale-dependent. Questions regarding the factors regulating oxygen availability at macro-to microscales, ranging from profiles and horizons to peds and microaggregates, and how to best represent them in models, warrants further research.

Finally, our results show that model estimates of bulk oxygen dynamics could be improved by considering OM bioavailability. In our system, OM bioavailability was a much stronger predictor of bulk oxygen concentrations than C content, microbial biomass, or microbial respiration. OM bioavailability in upland soils, as represented in current mechanistic model frameworks, is directly coupled to microbial respiration (Dwivedi et al., 2017; Riley et al., 2014). To fully capture the coupling between microbial respiration and oxygen availability, we suggest that microbial oxygen consumption needs to be directly linked to OM bioavailability.

5. Conclusions

In summary, we observed the existence of anoxic microsites in upland soils held at moderate moisture content, commonly used in many laboratory-based experiments (60% water filled pore space). While bulk oxygen concentrations ranged from 40 to 100% saturation, we observed significant micro-scale variability resulting in the formation of anoxic microsites. Anoxic microsites comprised 2 and 9% of the total soil volume, or 14–85% of the total pore volume. In our system, bulk oxygen concentrations were controlled by the amount of bioavailable OM supplying microbial respiration (and associated oxygen consumption) in macropores. In contrast, the extent of anoxic microsites was related to clay content, likely due to clay-rich domains in which micropore domains impose diffusion limitations. Our results suggest that oxygen diffusion limitations cause the formation of anoxic domains not only in cm-sized, saturated macroaggregates (Arah and Vinten, 1995; Sexstone et al., 1985) as assumed by current modeling approaches (Koven et al., 2013), but also at moderate moisture conditions within microaggregates. Anoxic microsites are known to regulate nutrient cycling (e.g., denitrification and Fe reduction) and have an increasingly recognized role as regulators of OM mineralization rates and C storage in soils (Hall and Silver, 2015; Keiluweit et al., 2016). In light of these results, further research into the dynamics of anoxic microsites and their impact on nutrient cycling and C storage in upland soils is warranted.

Acknowledgements

The authors thank M. Kleber and T. Wanzek for providing soil samples, D. Turner and G.-C. Li for help with soil characterization, and D. Parkinson and M. Voltolini for their support and assistance at the Advanced Light Source beamline 8.3.2. The Advanced Light Source is supported by the Director, Office of Science, Office of Basic Energy Sciences, of the U.S. DOE under Contract No. DE-AC02-05CH11231. A. Denney and K. Gee thank Stanford's Earth Summer Undergraduate Research (SESUR) and Summer Undergraduate Research in Geoscience and Engineering (SURGE) programs for support. This work was supported by the US Department of Energy, Office of Biological and Environmental Research, Terrestrial Ecosystem Program (Award Number DE-FG02-13ER65542). Finally, the authors thank three anonymous reviewers for their constructive comments.

Appendix A. Supplementary data

Supplementary data related to this article can be found at http://dx.doi.org/10.1016/j.soilbio.2017.12.002.

References

Arah, J.R.M., Smith, K.A., 1989. Steady-state denitrification in aggregated soils: a mathematical model. Journal of Soil Science 40, 139–149. http://dx.doi.org/10.1111/j.1365-2389.1989.tb01262.x.

Arah, J.R.M., Vinten, A.J.A., 1995. Simplified models of anoxia and denitrification in aggregated and simple-structured soils. European Journal of Soil Science 46, 507–517. http://dx.doi.org/10.1111/j.1365-2389.1995.tb01347.x.

Arndt, S., Jørgensen, B.B., LaRowe, D.E., Middelburg, J.J., Pancost, R.D., Regnier, P., 2013. Quantifying the degradation of organic matter in marine sediments: a review and synthesis. Earth-Science Reviews 123, 53–86. http://dx.doi.org/10.1016/j.earscirev.2013.02.008.

Bacher, M., Schwen, A., Koestel, J., 2015. Three-dimensional printing of macropore networks of an undisturbed soil sample. Vadose Zone Journal 14http://dx.doi.org/10.2136/vzj2014.08.0111. 0.

Bateman, E.J., Baggs, E.M., 2005. Contributions of nitrification and denitrification to N2O emissions from soils at different water-filled pore space. Biology and Fertility of Soils 41, 379–388. http://dx.doi.org/10.1007/s00374-005-0858-3.

Bundt, M., Widmer, F., Pesaro, M., Zeyer, J., Blaser, P., 2001. Preferential flow paths: biological 'hot spots' in soils. Soil Biology and Biochemistry 33, 729–738. http://dx.doi.org/10.1016/S0038-0717(00)00218-2.

Cotrufo, M.F., Soong, J.L., Horton, A.J., Campbell, E.E., Haddix, M.L., Wall, D.H., Parton, W.J., 2015. Formation of soil organic matter via biochemical and physical pathways of litter mass loss. Nature Geoscience 8, 776–779. http://dx.doi.org/10.1038/ngeo2520.

Currie, J., 1961. Gaseous diffusion in the aeration of aggregated soils. Soil Science 92, 40–45.

Davidson, EA, Samanta, S, Caramori, SS, Savage, K, 2012. The Dual Arrhenius and Michaelis-Menten kinetics model for decomposition of soil organic matter at hourly to seasonal time scales. Global Change Biol. 18, 371–384. http://dx.doi.org/10.1111/j.1365-2486.2011.02546.x.

Denef, K., Six, J., Merckx, R., Paustian, K., 2004. Carbon sequestration in microaggregates of No-Tillage soils with different clay mineralogy. Soil Science Society of America Journal 68, 1935–1944. http://dx.doi.org/10.2136/sssaj2004.1935.

Doube, M., Kłosowski, M.M., Arganda-Carreras, I., Cordelières, F.P., Dougherty, R.P., Jackson, J.S., Schmid, B., Hutchinson, J.R., Shefelbine, S.J., 2010. BoneJ: free and extensible bone image analysis in ImageJ. Bone 47, 1076–1079. http://dx.doi.org/10.1016/j.bone.2010.08.023.

Dwivedi, D., Riley, W.J., Torn, M.S., Spycher, N., Maggi, F., Tang, J.Y., 2017. Mineral properties, microbes, transport, and plant-input profiles control vertical distribution and age of soil carbon stocks. Soil Biology and Biochemistry 107, 244–259. http://dx.doi.org/10.1016/j.soilbio.2016.12.019.

Elberling, B., Askaer, L., Jørgensen, C.J., Joensen, H.P., Kühl, M., Glud, R.N., Lauritsen, F.R., 2011. Linking soil O2, CO2, and CH4 concentrations in a wetland soil: implications for CO2 and CH4 fluxes. Environmental Science & Technology 45, 3393–3399. http://dx.doi.org/10.1021/es103540k.

Fontaine, S., Barot, S., Barré, P., Bdioui, N., Mary, B., Rumpel, C., 2007. Stability of organic carbon in deep soil layers controlled by fresh carbon supply. Nature 450, 277–280. http://dx.doi.org/10.1038/nature06275.

Franzluebbers, A.J., 1999. Potential C and N mineralization and microbial biomass from

intact and increasingly disturbed soils of varying texture. Soil Biology and Biochemistry 31, 1083–1090. http://dx.doi.org/10.1016/S0038-0717(99)00022-X.
Freeman, C., Ostle, N., Kang, H., 2001. An enzymic "latch" on a global carbon store. Nature 409http://dx.doi.org/10.1038/35051650. 149–149.
Gottschalk, P., Smith, J.U., Wattenbach, M., Bellarby, J., Stehfest, E., Arnell, N., Osborn, T.J., Jones, C., Smith, P., 2012. How will organic carbon stocks in mineral soils evolve under future climate? Global projections using RothC for a range of climate change scenarios. Biogeosciences 9, 3151–3171. http://dx.doi.org/10.5194/bg-9-3151-2012.
Haberer, C.M., Rolle, M., Liu, S., Cirpka, O.A., Grathwohl, P., 2011. A high-resolution non-invasive approach to quantify oxygen transport across the capillary fringe and within the underlying groundwater. Journal of Contaminant Hydrology 122, 26–39. http://dx.doi.org/10.1016/j.jconhyd.2010.10.006.
Hall, S.J., Silver, W.L., 2015. Reducing conditions, reactive metals, and their interactions can explain spatial patterns of surface soil carbon in a humid tropical forest. Biogeochemistry 125, 149–165. http://dx.doi.org/10.1007/s10533-015-0120-5.
Hansel, C.M., Fendorf, S., Jardine, P.M., Francis, C.A., 2008. Changes in bacterial and archaeal community structure and functional diversity along a geochemically variable soil profile. Applied and Environmental Microbiology 74, 1620–1633. http://dx.doi.org/10.1128/AEM.01787-07.
Hedges, J.I., Keil, R.G., 1995. Sedimentary organic matter preservation: an assessment and speculative synthesis. Marine Chemistry 49, 81–115. http://dx.doi.org/10.1016/0304-4203(95)00008-F.
Jarvis, N.J., 2007. A review of non-equilibrium water flow and solute transport in soil macropores: principles, controlling factors and consequences for water quality. European Journal of Soil Science 58, 523–546. http://dx.doi.org/10.1111/j.1365-2389.2007.00915.x.
Keiluweit, M., Nico, P.S., Kleber, M., Fendorf, S., 2016. Are oxygen limitations under recognized regulators of organic carbon turnover in upland soils? Biogeochemistry 127, 157–171. http://dx.doi.org/10.1007/s10533-015-0180-6.
Keiluweit, M., Wanzek, T., Kleber, M., Nico, P., Fendorf, S., 2017. Anaerobic Microsites Have an Unaccounted Role in Soil Carbon Stabilization. Nature Communications. Nat. Commun. 8, 1771. http://dx.doi.org/10.1038/s41467-017-01406-6.
Kessel, V.,S.,J., Reeves, J.B., Meisinger, J.J., 2000. Nitrogen and carbon mineralization of potential manure components. Journal of Environmental Quality 29, 1669–1677. http://dx.doi.org/10.2134/jeq2000.00472425002900050039x.
Killham, K., Amato, M., Ladd, J.N., 1993. Effect of substrate location in soil and soil pore-water regime on carbon turnover. Soil Biology and Biochemistry 25, 57–62.
Klotzbücher, T., Kaiser, K., Guggenberger, G., Gatzek, C., Kalbitz, K., 2011. A new conceptual model for the fate of lignin in decomposing plant litter. Ecology 92, 1052–1062. http://dx.doi.org/10.1890/10-1307.1.
Köchy, M., Hiederer, R., Freibauer, A., 2015. Global distribution of soil organic carbon – Part 1: masses and frequency distributions of SOC stocks for the tropics, permafrost regions, wetlands, and the world. SOIL 1, 351–365. http://dx.doi.org/10.5194/soil-1-351-2015.
Koven, C.D., Riley, W.J., Subin, Z.M., Tang, J.Y., Torn, M.S., Collins, W.D., Bonan, G.B., Lawrence, D.M., Swenson, S.C., 2013. The effect of vertically resolved soil biogeochemistry and alternate soil C and N models on C dynamics of CLM4. Biogeosciences 10, 7109–7131. http://dx.doi.org/10.5194/bg-10-7109-2013.
Leffelaar, P.A., 1988. Dynamics of partial anaerobiosis, denitrification, and water in a soil aggregate: simulation. Soil Science 146, 427–444.
Lehmann, J., Kinyangi, J., Solomon, D., 2007. Organic matter stabilization in soil microaggregates: implications from spatial heterogeneity of organic carbon contents and carbon forms. Biogeochemistry 85, 45–57. http://dx.doi.org/10.1007/s10533-007-9105-3.
Linn, D.M., Doran, J.W., 1984. Effect of water-filled pore space on carbon dioxide and nitrous oxide production in tilled and nontilled Soils1. Soil Science Society of America Journal 48, 1267. http://dx.doi.org/10.2136/sssaj1984.03615995004800060013x.
MacDowell, A.A., Parkinson, D.Y., Haboub, A., Schaible, E., Nasiatka, J.R., Yee, C.A., Jameson, J.R., Ajo-Franklin, J.B., Brodersen, C.R., McElrone, A.J., 2012. X-ray Microtomography at the Advanced Light Source. http://dx.doi.org/10.1117/12.930243. 850618–850618–14.
Megonigal, J.P., Hines, M.E., Visscher, P.T., 2003. Anaerobic metabolism: linkages to trace gases and aerobic processes. In: Holland, H.D., Turekian, K.K. (Eds.), Treatise on Geochemistry. Pergamon, Oxford, pp. 317–424.
Moyano, F.E., Manzoni, S., Chenu, C., 2013. Responses of soil heterotrophic respiration to moisture availability: an exploration of processes and models. Soil Biology and Biochemistry 59, 72–85. http://dx.doi.org/10.1016/j.soilbio.2013.01.002.
Moyano, F.E., Vasilyeva, N., Bouckaert, L., Cook, F., Craine, J., Curiel Yuste, J., Don, A., Epron, D., Formanek, P., Franzluebbers, A., Ilstedt, U., Kätterer, T., Orchard, V., Reichstein, M., Rey, A., Ruamps, L., Subke, J.-A., Thomsen, I.K., Chenu, C., 2012. The moisture response of soil heterotrophic respiration: interaction with soil properties. Biogeosciences 9, 1173–1182. http://dx.doi.org/10.5194/bg-9-1173-2012.
Myrold, D.D., 1988. Denitrification in ryegrass and winter wheat cropping systems of western Oregon. Soil Science Society of America Journal 52, 412. http://dx.doi.org/10.2136/sssaj1988.03615995005200020019x.
Nie, M., Pendall, E., Bell, C., Wallenstein, M.D., 2014. Soil aggregate size distribution mediates microbial climate change feedbacks. Soil Biology and Biochemistry 68, 357–365. http://dx.doi.org/10.1016/j.soilbio.2013.10.012.
Nielson, K.K., Rogers, V.C., Gee, G.W., 1984. Diffusion of radon through soils: a pore distribution Model1. Soil Science Society of America Journal 48, 482. http://dx.doi.org/10.2136/sssaj1984.03615995004800030002x.
Oades, J.M., 1988. The retention of organic matter in soils. Biogeochemistry 5, 35–70. http://dx.doi.org/10.1007/BF02180317.
Parton, W.J., Hartman, M., Ojima, D., Schimel, D., 1998. DAYCENT and its land surface submodel: description and testing. Global and Planetary Change 19, 35–48.
Plante, A.F., Conant, R.T., Stewart, C.E., Paustian, K., Six, J., 2006. Impact of soil texture on the distribution of soil organic matter in physical and chemical fractions. Soil Science Society of America Journal 70, 287. http://dx.doi.org/10.2136/sssaj2004.0363.
Reddy, K.R., D'Angelo, E.M., Harris, W.G., 2000. Biogeochemistry of wetlands. In: Sumner, M.E. (Ed.), Handbook of Soil Science, pp. G89–G119.
Reddy, K.R., Feijtel Jr., T.C., Patrick, W.H., 1986. Effect of soil redox conditions on microbial oxidation of organic matter. In: Chen, Y., Avnimelech, Y. (Eds.), The Role of Organic Matter in Modern Agriculture, Developments in Plant and Soil Sciences. Springer, Netherlands, pp. 117–156.
Riley, W.J., Maggi, F.M., Kleber, M., Torn, M.S., Tang, J.Y., Dwivedi, D., Guerry, N., 2014. Long residence times of rapidly decomposable soil organic matter: application of a multi-phase, multi-component, and vertically-resolved model (TOUGHREACTv1) to soil carbon dynamics. Geoscientific Model Development Discussions 7, 815–870. http://dx.doi.org/10.5194/gmdd-7-815-2014.
Sexstone, A.J., Revsbech, N.P., Parkin, T.B., Tiedje, J.M., 1985. Direct measurement of oxygen profiles and denitrification rates in soil Aggregates1. Soil Science Society of America Journal 49, 645. http://dx.doi.org/10.2136/sssaj1985.03615995004900030024x.
Sierra, CA, Malghani, S, Loescher, HW, 2017. Interactions among temperature, moisture, and oxygen concentrations in controlling decomposition rates in a boreal forest soil. Biogeosciences 14, 703–710. http://dx.doi.org/10.5194/bg-14-703-2017.
Six, J., Bossuyt, H., Degryze, S., Denef, K., 2004. A history of research on the link between (micro)aggregates, soil biota, and soil organic matter dynamics. Soil and Tillage Research 79, 7–31. http://dx.doi.org/10.1016/j.still.2004.03.008.
Sleutel, S., De Neve, S., Prat Roibás, M.R., Hofman, G., 2005. The influence of model type and incubation time on the estimation of stable organic carbon in organic materials. European Journal of Soil Science 56, 505–514. http://dx.doi.org/10.1111/j.1365-2389.2004.00685.x.
Stookey, L.L., 1970. Ferrozine—a new spectrophotometric reagent for iron. Analytical Chemistry 42, 779–781. http://dx.doi.org/10.1021/ac60289a016.
Torn, M.S., Trumbore, S.E., Chadwick, O.A., Vitousek, P.M., Hendricks, D.M., 1997. Mineral control of soil organic carbon storage and turnover. Nature 389, 170–173. http://dx.doi.org/10.1038/38260.
Torn, M.S., Vitousek, P.M., Trumbore, S.E., 2005. The influence of nutrient availability on soil organic matter turnover estimated by incubations and radiocarbon modeling. Ecosystems 8, 352–372. http://dx.doi.org/10.1007/s10021-004-0259-8.
Totsche, K.U., Amelung, W., Gerzabek, M.H., Guggenberger, G., Klumpp, E., Knief, C., Lehndorff, E., Mikutta, R., Peth, S., Prechtel, A., Ray, N., Kögel-Knabner, I., 2017. Microaggregates in soils. Journal of Plant Nutrition and Soil Science 000, 1–33. http://dx.doi.org/10.1002/jpln.201600451.
Veen, J.A.V., Kuikman, P.J., 1990. Soil structural aspects of decomposition of organic matter by micro-organisms. Biogeochemistry 11, 213–233. http://dx.doi.org/10.1007/BF00004497.
Zhuang, J., McCarthy, J.F., Perfect, E., Mayer, L.M., Jastrow, J.D., 2008. Soil water hysteresis in water-stable microaggregates as affected by organic matter. Soil Science Society of America Journal 72, 212. http://dx.doi.org/10.2136/sssaj2007.0001S6.